COMPARISON OF VARIOUS METHODS FOR ESTIMATING WAVE INCIDENT ANGLES IN THE NEARSHORE ZONE

AS Ngusaru
Institute of Marine Sciences, University of Dar es Salaam
P.O. Box 668, Zanzibar

ABSTRACT

Five different methods were examined for their suitability in estimating the inshore wave incident angles on a nearshore zone with a complex topography. Visual observation provided preliminary estimates. Two frequency independent methods and one frequency dependent method based on current meter measurements were examined. Another frequency dependent method based on collocated bottom pressure and current meter measurements was also examined. The results from all the methods provided a reasonably consistent estimate of the inshore wave incident angles. The frequency independent methods gave exactly the same results while the frequency dependent methods had a 5% relative error among themselves. Between frequency independent and frequency dependent methods, the relative error was 11%. However, since the frequency dependent methods involve smoothing of the velocity spectra, this method was found to be rather subjective. The frequency independent method based on high passed velocity vectors seems to be easy to apply and to provide unambiguous estimate of inshore wave incident angles.

INTRODUCTION

Surface waves are often observed to be constantly forming offshore, then travel for a short distance before breaking at the nearshore zone. Measurement and prediction of these waves are important in many of today's concerns. For example, in planning shipping routes, estimating storm damage risks, and driving amounts of coastal erosion. Global models of directional wave spectra are routinely run to assist in these endeavours. Local inshore wave incident conditions are crucial inputs for the coastal evolution (Wright *et al.* 1985, Kamphuis 1993, Rosati *et al.* 1993, Niedoroda *et al.* 1995) and shoreline processes models (Thornton & Guza 1989, Dabees & Kamphuis 1997). Incident wave angles are also used in modelling the nearshore horizontal current velocities using contemporary theories (Ryrie 1983, Kamphuis 1991, Kobayashi & Karjadi 1994). However, a model is only as good as the

information going into it. Ocean waves, particularly the inshore direction of wave propagation can be very tricky to measure. The wave transformation processes determine local wave incident conditions. In deep water, the water particle motion due to waves is confined to the vicinity of the surface. Therefore, bottom friction has no appreciable effect on wave motion. In shallower areas, the wave transformation is under the influence of both the sloping bottom and bottom roughness. This transformation due to shoaling processes has been described by many authors (e.g. Horikawa 1988, Thornton & Guza 1983). The waves are first observed to be decreasing and then gradually increase in height, maintaining symmetrical fronts and rear faces. With further decrease in water depth, the wave height increases rapidly to produce an asymmetrical wave profile, and finally it breaks. The energy dissipation associated with wave breaking result in a wave set-up on gently sloping beaches and also contributes as the driving force for the horizontal nearshore currents (Guza & Thornton 1981, Kobayashi & Wurjanto 1992). Figure 1 shows a schematic plan of a wave approaching the breaker line on a shore with a gentle slope. Figure 2 shows a schematic plan of the incoming wave to a nearshore zone characterized by multiple wave breakers and the generated longshore currents. Rip currents are often generated when longshore currents of opposite direction coincide at one location, causing offshore jets of water, which are often dangerous to swimmers in natural beaches (Smith & Largier 1995, Haller *et al.* 1998). Since waves travel more slowly over shallow water than over deep water, the inshore part of the long wave crest is more retarded than the part further away. Therefore, if a series of parallel-crested waves approach at an angle to a straight shoreline over a smooth sea bottom which shoals gradually, they progressively change direction as the end of the wave nearer to the shore slows down earlier than that farther away. As a result, the waves become more parallel to the shore by the time they pile up as surf. This means that waves are also subject to refraction. If the sea bottom does not have a uniform slope along the full length of the shore, the refraction may be more complicated.

There have been many suggestions on how to measure the deep-water wave incident conditions. Traditionally the directional wave buoys (up to 1m diameter) are used as surface following buoys that can measure horizontal and vertical orbital displacements at the sea surface, from which wave height spectra and directional wave properties can be determined (Komen 1994). Recently, directional waverider buoys have been developed with directional resolution of 1.5°. Wave angles can also be measured using spatial information, for example remote sensing of ocean waves by Synthetics Aperture Radar (Marom *et al.* 1990). However, the main focus of the present paper is on the use of moored instruments to measure the inshore wave incident angles. These instruments are most accessible by many marine scientists working in the nearshore zone and can provide reliable source of information on the inshore waves incident conditions.

A number of classic techniques exist for estimating inshore wave incident angles using moored instruments (e.g. Fofonoff 1969, Aubrey & Spencer 1983). Todate, there have been very few attempts to test the techniques using field data collected from nearshore areas with complicated bathymetry. It is therefore interesting to examine five of the commonly applied methods using field data that was obtained from a site characterized by a multi-barred system. The incident angle measured using the methods described here is normally independent of the geographic location or the season of the year, thus the methods might be applicable in any nearshore zone.

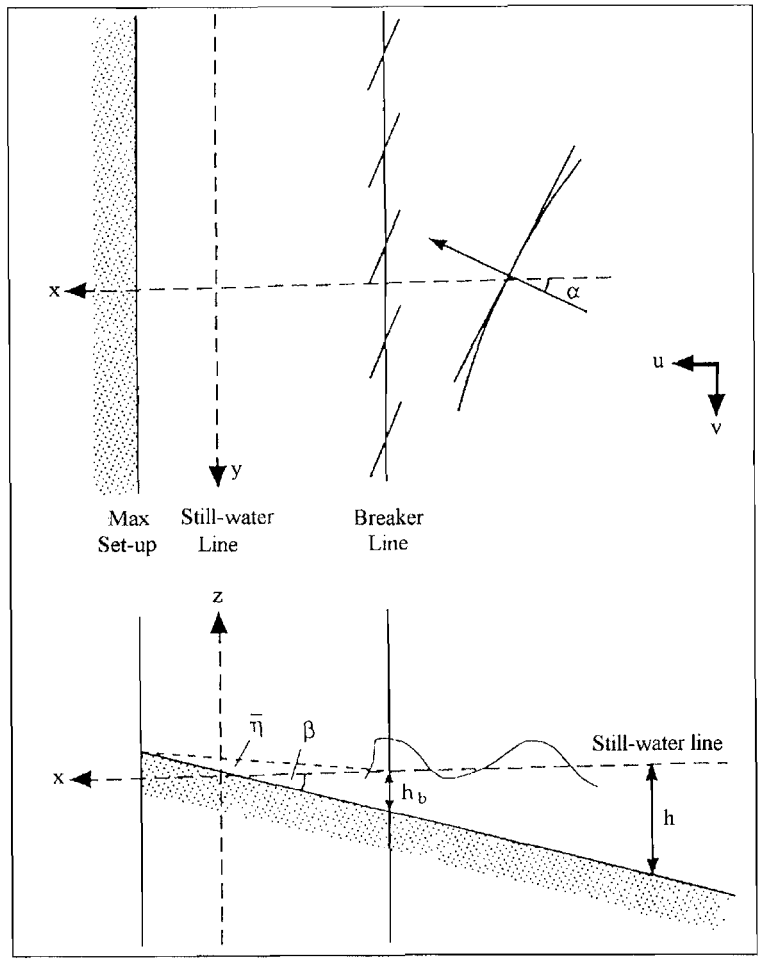

Fig. 1: Schematic plan showing the incident wave and subsequent breaking in the nearshore zone. The still-water line indicates the mean water level and the max set-up indicates the elevation of water level at the beach due to the momentum associated with wave breaking. The wave-orbital velocity vector is resolved into the alongshore (v) and cross-shore velocity (u).

METHODS

Inshore wave incident angles can in principle be estimated using visual estimation, or using frequency dependent or frequency independent methods. Two useful methods independent of frequency are the scatter diagram and a classic method suggested by Fofonoff (1969). The other two classic frequency dependent methods include a method suggested by Fofonoff (1969) and one based on the use of collocated Electromagnetic Current Meter (ECM) and bottom pressure sensor suggested by Aubrey and Spencer (1983)

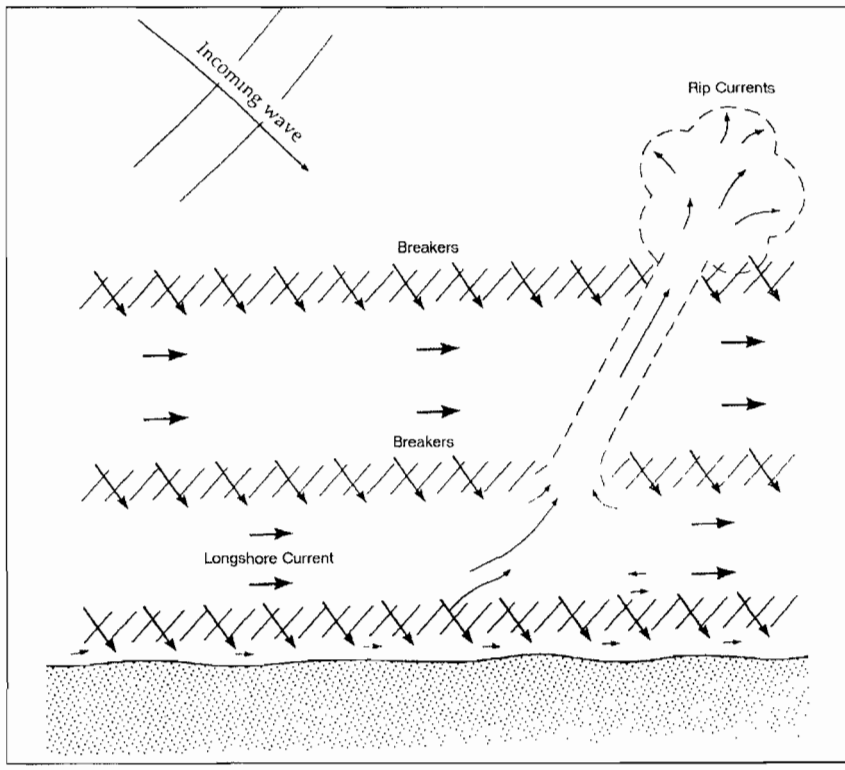

Fig. 2: Schematic plan of longshore are rip currents generated by breaking waves. The magnitude of the generated longshore currents depends on the angle of the incoming waves

The data set used here is based on the much larger field campaign that was carried out at Stanhope Lane beach in Prince Edward Island as part of the Canadian Coastal Sediment Study (C^2S^2) experiment. The beach was relatively straight with a gentle slope of about 0.018. The average breaker height was 0.5 m and a typical peak frequency of incident waves (f_p) was 0.14 Hz. Tidal range was about 0.7 m for spring tides and 0.4 m for neap tides.

The bottom topography was characterized by a well-developed multi-bar system. Three linear bars located at 100 m, 200 m and 400 m offshore were entirely within the surf zone during the period of experiment (Fig. 3). A dense array of Marsh-Mcbirney bi-directional recording current meters and bottom pressure sensors were deployed on a line oriented perpendicular to the shoreline to measure the cross-shore distribution of the flow field and the deep water incident wave conditions. The main purpose of the experiment was to investigate theoretical modelling of longshore currents. Since the measurements were taken simultaneously, it was possible to investigate both the modelling of these currents and the inshore wave incident conditions over a multi-barred beach using a comprehensive data set.

Underwater data acquisition system (UDATS) was used to obtain the bottom pressure and record the flow field (Hazen *et al.* 1987). Six main stations were set-up for the cross-shore deployment of instruments, which included current meters, bottom pressure sensors and a tide gauge. The bottom profile and the position of the bars at the time of instruments deployment are shown in Figure 3. A pressure sensor and a Marsh-Mcbiney electromagnetic current meter (EMC) were positioned on the first station at the seaward side of the bar. The bottom pressure sensors and EMC's were positioned nominally at 20 cm above the bed. The second station was located in the trough between the first and the middle bar.

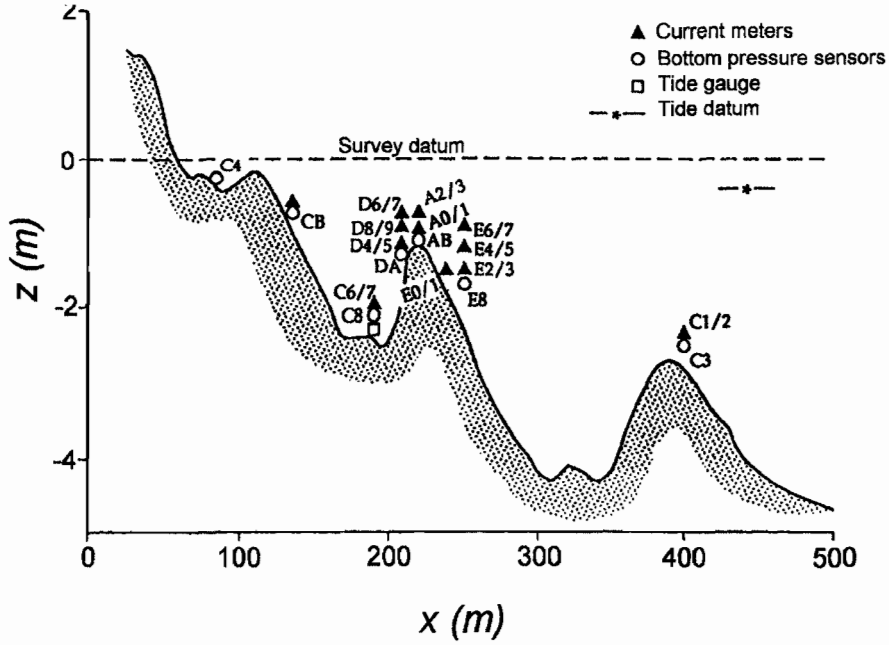

Fig. 3: Nearshore profile showing a well developed multi-bar system and the inshore moored instruments deployed at distances of 80 m, 190 m, 220 m, 250 m and 400 m. The first and second numbers in the current meters indicate the cross-shore and alongshore velocity channels respectively

A pressure sensor, one EMC and a tide gauge were positioned here at 45 cm above the bed. Three stations were located on the middle bar where a dense concentration of instruments was deployed. The instruments here included bottom pressure sensors and EMC's. The sixth station was located on the third bar where one pressure sensor and one EMC were deployed at the top of the bar. Further pressure gauges were deployed close to the shore in the water that was too shallow particularly during the low tides, to allow deployment of other instruments. A wave directional buoy was also deployed at about 3.5 km offshore to record the deep-water wave conditions. A standard 10 m meteorological tower was erected approximately 45 m landward from the edge of the cliff and 50 m west of the main instrument mooring line to measure wind speed and direction, humidity and barometric pressure.

Data runs were started when winds picked up to examine the development from calm conditions to high waves and strong wave breaking conditions. EMC's and pressure gauges were connected by cable to the data acquisition computer at the shore station. Sampling was performed at 4.55 Hz and data were collected hourly during wind events and every 90 minutes during build up and decay periods. At high frequency, the measurements of the cross-shore current gave the amplitude of the horizontal on-offshore wave-orbital velocities. The instantaneous wave orbital velocity time series were then averaged over 5 minutes to obtain the mean and standard deviations. The instantaneous longshore velocity was obtained as a sum of the longshore component of the wave-orbital velocity, mean longshore velocity and any other long or shear wave activity.

The flow sensors deployed at 400-m offshore where waves were breaking over the bar were used in the analysis presented in this paper. The results on field measurements and modelling of long-shore currents over a multi-barred beach using this data set are presented elsewhere (Ngusaru 2000).

Method 1: Visual estimation

Visual observation, despite being the crudest method for estimating the angles of incoming waves, is still used for preliminary determinations of wave angles. However, in order to obtain a time series of incident angles over longer time periods, more sophisticated methods of estimating wave incident angles using self-recording instruments are necessary. In this paper, the preliminary wave incident angles were visually estimated by observing waves breaking on a bar located at about 400-m offshore. The wave angles obtained were compiled in a logbook throughout the days in which observations were made.

Method 2: Frequency Independent Method-1

From the theory of waves for small amplitudes we have

$$v = u\tan\alpha \qquad (1)$$

where α is the wave incident angle, $u(t)$ and $v(t)$, respectively, are the half-hour time series of cross-shore and long-shore components of the current velocity vector field in Eulerian form. From Equation (1) we obtain α as the slope of the scatter plot of u against v. The values of u and v for October 23, 1989 were measured using the bi-directional electromagnetic recording current meter as elaborated above. The scatter plot method depends on the tendency of the orbital current fluctuations to have preferred orientation. The tendency is quantified by computing the principal axes of the scatter plot from the cross-shore and along-shore current statistics. The main features of the scatter plot reveal a major axis that lies along the direction of maximum current variance and minor axis normal to it. The estimate of incident angle is obtained by measuring the angle between the major axis and the horizontal axis of the plot. However, there are cases where the scatter diagrams show a weaker preferred orientation. In this case the method cannot be useful for estimating the wave incident angles and indicate the uncertainty associated with the method.

Method 3: Frequency Independent Method-2

The second frequency independent method for estimating wave incident angles was suggested by Fofonoff (1969), where a classical relation for the wave incident angle was derived:

$$\alpha = \frac{1}{2}\tan^{-1}\left[\frac{2\langle u'v'\rangle}{\langle u'^2\rangle - \langle v'^2\rangle}\right] \qquad (2)$$

where

$$\mathbf{u}' = \mathbf{u} - \langle \mathbf{u} \rangle$$

$$\mathbf{v}' = \mathbf{v} - \langle \mathbf{v} \rangle$$

The angle brackets < > indicate a half-hour velocity averaging to obtain the low frequency values. Similarly, (**u'**, **v'**) and (**<u>**, **<v>**) are respectively, the high frequency and the time averaged velocity components. This approach is particularly interesting because similarity parameters are also used in calculation of the $\mathbf{S_{xy}}$ component of the radiation stress (Equation 3), which is a classic forcing for horizontal nearshore currents (Longuet-Higgins 1964).

$$S_{xy} = \rho h\langle u'v'\rangle \qquad (3)$$

where like in Equation (2), **u'** and **v'** represent the high pass velocity components and (ρ,**h**) are, respectively, water density and depth.

As described above, the values of **u(t)** and **v(t)** were measured as half-hour time series at sampling frequency of 4.55 Hz. Following Guza and Thornton (1985), the values of **<u'v'>** in Equation (2) were obtained by multiplying the high frequency velocity components and then taking the half-hour time average of the product. Similarly the values of **<u'^{2}>** and **<v'^{2}>** were obtained by taking the square of the high frequency velocity components before averaging to obtain the half-hour mean values.

Method 4: Frequency dependent method-1

The first frequency dependent method for determining wave incident angles was suggested by Fofonoff (1969) using the spectral analysis of vector series. The **u(t)** and **v(t)** components of velocity vector are two related time series that can be examined by standard spectral methods. Since the velocity vector is resolved along arbitrary axes, the two components are not independent. Therefore the auto and cross-correlation and the spectral functions that are generated becomes important tools in analyzing the velocity vector records. Based on Fofonoff (1969), α can be obtained from

$$\alpha = \frac{1}{2}\tan^{-1}\left[\frac{2C_{uv}}{P_{uu} - P_{vv}}\right] \qquad (4)$$

where $\mathbf{C_{uv}}$ is the co-spectrum (the real part of the cross-spectrum), while $\mathbf{P_{uu}}$ and $\mathbf{P_{vv}}$ are the auto-spectra defined by:

$$C_{uv} = R_e(u^* \bar{v})$$

$$P_{uu} = u^* \bar{u}$$

$$P_{vv} = v^* \bar{v}$$

where $\overline{(\,)}$ and $(\,)^*$ respectively denote mean and complex conjugates.

Method 5: Frequency dependent method-2

The second frequency dependent method for determination of wave incident angle requires collocated pressure and current meter measurements (Aubrey and Spencer, 1983). A collocated pressure sensor deployed in the third bar near the position of the Electromagnetic current meter was therefore used in this analysis. The pressure sensor measured the sum of hydrostatic and dynamic pressure (**p**). The wave angle of incidence was then estimated by:

$$\alpha = \frac{1}{2}\tan^{-1}\left[\frac{2C_{pv}}{P_{pu}}\right] \qquad (5)$$

where $\mathbf{C_{pv}}$ and $\mathbf{C_{pu}}$ represent the co-spectrum for **p,v** and **p,u** measurements respectively.

In the present paper, the spectral functions in the frequency dependent methods discussed above were determined using the cross-spectrum and auto-spectra signal processing subroutine of the MATLAB (Moller *et al.* 1989), which is a high-performance interactive software package for scientific and engineering numeric computation.

RESULTS AND DISCUSSION

Visual estimates

Generally, on October 23, the waves were visually observed to be breaking over the third bar (Fig. 3) at about 20° (Table 1). This preliminary angle was then compared with the wave angles that were determined based on measurements obtained using moored bottom pressure gauge and a current meter deployed on that bar. The measurements and visual estimates were taken simultaneously.

Table 1: Summary of the estimated wave angle of incidence α (°) using five different methods, where FI and FD are respectively the frequency independent and frequency dependent methods

Method	Visual	FI1	FI2	FD1	FD2
α(°)	20	14	14	12.6	13.2

Frequency independent method-1

Figure 4 shows the scatter diagram obtained using the half-hour time series of **u,v** data as measured by the bi-directional current meter over the third bar in

October 23. The angle between the principal axis and the horizontal axis of this plot gave the wave incident angle of $\alpha = 14^{o}$.

Frequency independent method-2

The second frequency independent method was also evaluated using the same half-hour **u,v** time series data shown in the scatter plot (Fig. 4). The calculation using this method gave

$$\langle u'v' \rangle = 0.0544$$

and

$$\langle u'^2 \rangle - \langle v'^2 \rangle = 0.2047$$

The computed angle is therefore

$$\alpha = \frac{1}{2}\tan^{-1}\left[\frac{2*0.0544}{0.2047}\right] = 14.0^{\circ}$$

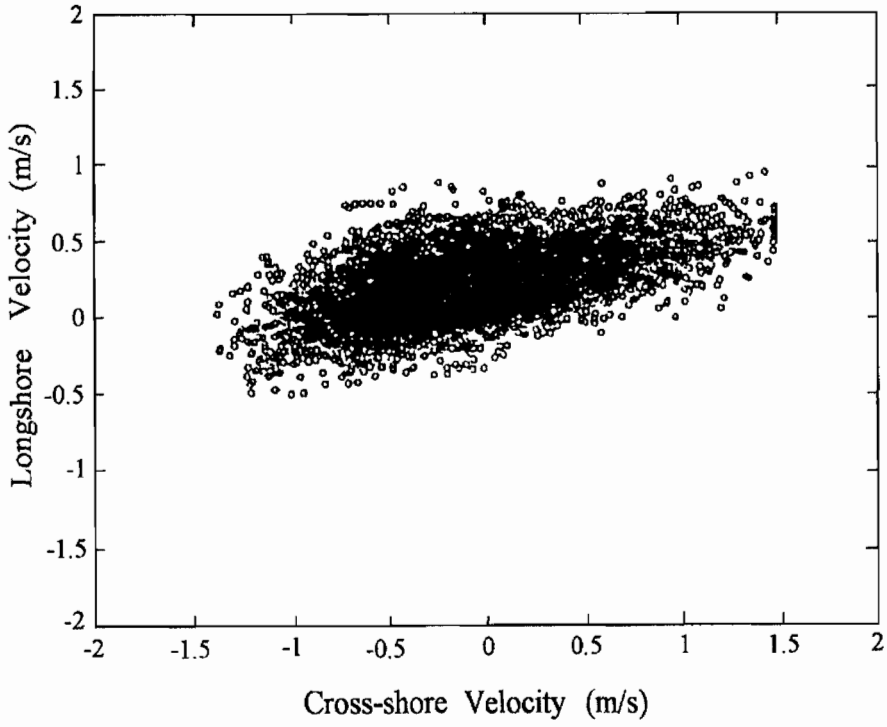

Fig. 4: Scatter diagram of the cross-shore velocities (u) against alongshore velocities (v) for October 23 showing preferred orientation, Prince Edward Island, 1989.

Frequency dependent method-1

Equation (4) was used to calculate the wave incident angles using the first frequency dependent method, based on the **u,v** velocity data shown in Figure 3. The spectra functions given in Equation (4) are clearly frequency dependent, therefore the computed angles are also a function of frequency. It is therefore necessary to evaluate the estimated wave incident angle at the peak frequency. The reason behind the use of the peak frequency is that the enhanced spectral peak contributes a substantial amount of the total variance or energy in the spectrum. The peak frequency represents the dominant oscillations and is therefore a sensitive indicator of the part of the spectrum where significant power is concentrated; the low and high-frequency tails of the spectrum represent the harmonics.

The computed autospectra $\mathbf{P_{uu}}$ and $\mathbf{P_{vv}}$, the co-spectrum ($\mathbf{C_{uv}}$) and quadrature spectrum ($\mathbf{Q_{uv}}$) are shown in Figure 5. The values obtained at the peak frequency for these spectral functions are, $\mathbf{C_{uv}}$=0.526 and $\mathbf{P_{uu}}$-$\mathbf{P_{vv}}$=2.33. Therefore the computed angle is

$$\alpha = \frac{1}{2}\tan^{-1}\left[\frac{2*0.526}{2.23}\right] = 12.6^{\circ}$$

Small changes of the computed incident angle were noticed when using various filters in the spectral analysis. Figure 6 shows the smoothing effect of the computed spectrum associated with changing the filter coefficients.

Frequency dependent method-2

The computation of wave incident angle using the collocated pressure sensor and current meter measurements is given below, where $\mathbf{C_{pu}}$, $\mathbf{Q_{pu}}$, $\mathbf{C_{pv}}$ and $\mathbf{Q_{pv}}$ are shown in Figure 7. The values obtained are $\mathbf{C_{pu}}$=0.98, $\mathbf{Q_{pu}}$=0.30, $\mathbf{C_{pv}}$=0.23 and $\mathbf{Q_{pv}}$=0.098. Therefore the computed angle is

$$\alpha = \frac{1}{2}\tan^{-1}\left[\frac{0.23}{0.98}\right] = 13.2^{\circ}$$

All the examined methods using moored instruments gave reasonably consistent estimation of the wave incident angles. However, the estimation using visual observation seems to have overestimated the wave incident angle. The estimated α =20° is in this analysis treated as an outlier. This method should therefore be used for preliminary purposes only, or in investigations that do not require high accuracy in the estimated wave incident angles. The frequency independent methods gave exactly the same results while the frequency dependent methods had a 5% relative error among themselves.

Between frequency independent and frequency dependent methods the relative error was 11%.

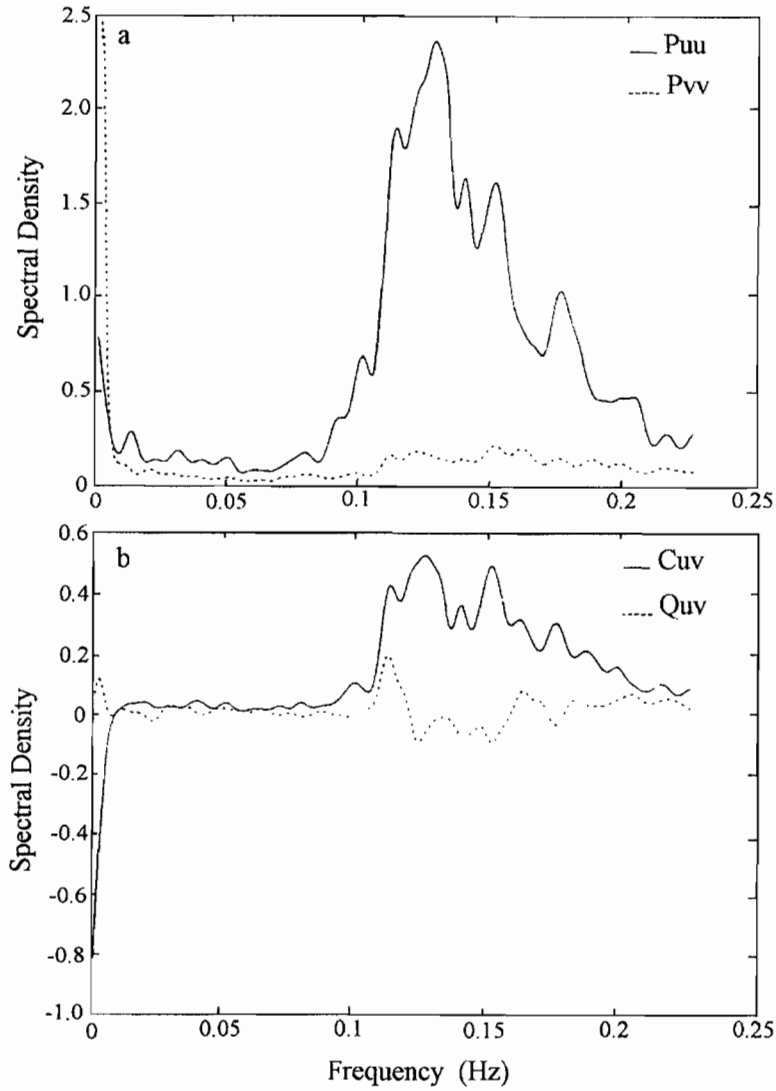

Fig. 5: Auto-spectra P_{uu} and P_{vv}, Co-spectrum C_{uv} and Quadrature spectrum Q_{uv} for the velocity data shown in Figure 3 as used in computing the wave incident angles based on frequency dependent method using current meter measurements

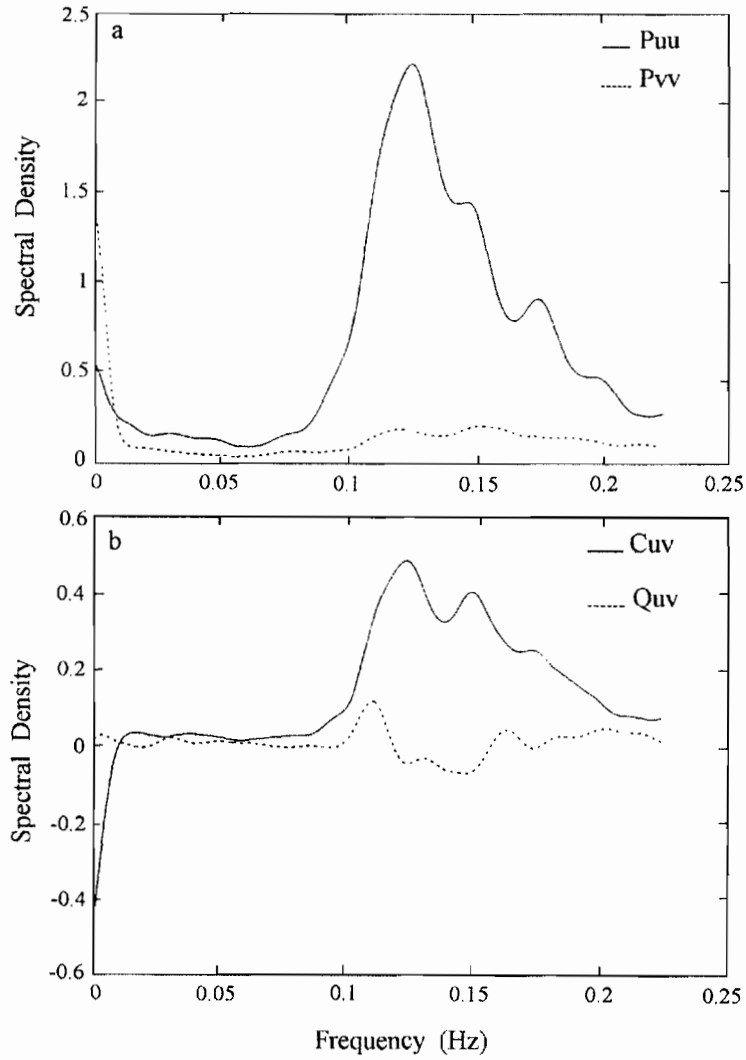

Fig. 6: Auto-spectra P_{uu} and P_{vv}, Co-spectrum C_{uv} and Quadrature spectrum Q_{uv} for the velocity data shown in Figure 5, but using a filter with slightly different coefficient

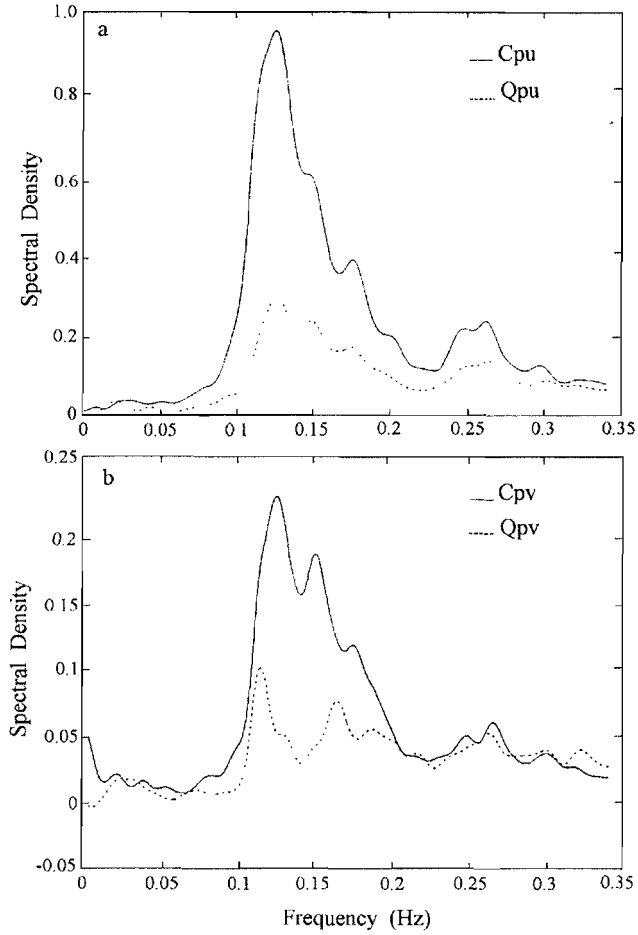

Fig. 7: Co-spectrum C_{pu}, C_{pv} and Quadrature spectrum Q_{pu}, Q_{pv} for the velocity data shown in Figure 3 as used in computing the wave incident angles based on frequency dependent method using collocated bottom pressure and current meter measurements

Since there was no other independent and more reliable measurement of the wave incident angles at the third bar, one cannot easily conclude on the accuracy of the methods. A directional buoy at the location of moored instruments would have provided the exact angle of the incident waves. However, it was not the intension of the current work to discuss the details of the accuracy of the individual methods. More work is recommended on statistical analysis to evaluate the accuracy of the methods. The main aim here was to compare the results obtained using the methods and the potential for their application in

nearshore areas with complex bottom topography. The results shows that, the frequency dependent methods involving spectral analysis of velocity vectors require smoothing or averaging of the velocities in order to determine a representative angle. Therefore the reliability of these methods depends on the smoothing operation that is rather subjective. This method should therefore be applied with caution. Similarly, the scatter plot method depends on the tendency of the wave orbital velocity fluctuations to have preferred orientations. In cases where the measured velocities show weak preferred orientation, the scatter plot method may give uncertain results. The frequency independent method based on high passed velocity vectors seems to be easy to apply and provide unambiguous estimate of inshore wave incident angles.

ACKNOWLEDGEMENT

The author would like to thank the anonymous reviewers for their comments and Professor AJ Bowen for the support and encouragement. The experiment described here was partly sponsored by the Natural Science and Engineering Research Council of Canada. Further financial support was provided by the International Center for Ocean Development (ICOD).

REFERENCES

Aubrey DG and Spencer WD 1983 *Canadian coastal sediment study (C^2S^2). Inner shelf sand transport and wave measurements, Pointe Sapin, New Brunswick, Canada.* Woods Hole Oceanographic Institution Report No. C^2S^2-5

Dabees MA and Kamphuis JW 1997 *Numerical modeling and coastal processes: overview of a modeling system for simulating shoreline change.* Proc., Canadian Coastal Conf. Guelph, Canada, 161-176

Fofonoff NP 1969 Spectral characteristics of internal waves in the ocean. *Deep Sea Research Supplement* **16**: 58-71

Guza RT and Thornton EB 1981 Wave set-up on a natural beach. *Journal of Geopgysical Research* **86**: 4133-4137

Guza RT and Thornton EB 1985 Velocity moments in the nearshore. *Journal of Waterways, Harbours and Coastal Engineering* **111**: 235-256

Haller MC, Dalrymple RD and Svendsen IA 1998 Rip channels and nearshore circulation. *Coastal Dynamics* **97**: 594-603

Hazen DG, Huntley D and Bowen AJ 1987 *UDATS: A system for measuring nearshore processes.* Proc. Oceans '87 Conference, Halifax

Horikawa K 1988 *Nearshore dynamics and coastal processes: Theory, measurement and predictive models.* University of Tokyo Press

Kamphuis JW 1991 Alongshore Sediment Transport Rate. *Journal of Waterway, Port and Coastal Ocean Engineering.* **ASCE**. 624-640

Kamphuis JW 1993 *Effective modeling of coastal morphology.* Proc., 11th Australian Conf. on Coastal and Ocean Eng. Institution of Engineers of Australia

Kobayashi N and Karjadi EA 1994 S*wash dynamics under obliquely incident waves*. International Proceeding of Coastal Engineering 2155-2169

Kobayashi N and Wurjanto A 1992 Irregular wave setup and run-up on beaches. *Journal of Water Port Coastal Ocean Engineering* **115**: 368-386

Komen GL 1994 Sea surface winds and atmospheric circulation. In: Komen GL, Cavaleri L, Donelan M, Hasselmann K, Hasselmann S and Janssen PAEM (eds): *Dynamics and modeling of ocean waves*. Cambridge University Press

Longuet-Higgins MS 1964 Radiation stresses in water waves: a physical discussion with application. *Deep-Sea Research* **11**: 529-562

Marom MR, Goldstein M, Thornton EB and Shemer L 1990 Remote Sensing of Ocean Waves by Interferometric SAR. *Nature* **345**: 793-795

Moler C, Little J and Bangert S 1988 *Pro-Matlab for VAX/VMS computers, users guide*. The Math Works Inc

Ngusaru AS 2000 Longshore currents over a multi-barred beach: field measurements and dissipation models. *Indian Journal of Marine Sciences* **29**: 206-218

Niedoroda AW, Reed CW, Swift DJP, Arato H and Hoyanagi K 1995 Modeling shore-normal large-scale coastal evolution. *Marine Geology*, **126**: 181-199

Rosati JD, Wise RA, Kraus NC and Larson M 1993 *SBEACH: Numerical model for simulating storm-induced beach change*. Report 3: User's manual. Instruction Report CERC-93-2, Coastal Engineering Research Center

Ryrie SC 1983 Longshore motion generated on beaches by obliquely incident bores. *Journal of Fluid Mechanics* **129**: 193-212

Smith JA and JLargier L 1995 Observations of nearshore circulation: Rip currents. *Journal of Geophysical Research* **100 (C6)**: 10967-10975

Thornton EB and Guza RT 1983 Transformation of wave height distribution. *Journal of Geophysical Research* **88 (C10)**: 5925-5938

Thornton EB and Guza RT 1989 Nearshore sediment transport, In: Seymour RJ (ed) *Models for surf zone dynamics*. Plenum Press, New York, pp. 337- 370

Wright LD, Short AD and Green MO 1985 Short-term changes in the morphodynamic states of beaches and surf zones: an empirical predictive model. *Marine Geology* **62**: 339-364